

NONLINEAR OPTICAL PHENOMENA https://doi.org/10.1070/QEL17198

Multifrequency stimulated Raman scattering of light in a calcite single crystal

V.S. Gorelik, A.V. Skrabatun, V.A. Orlovich, A.I. Vodchits

Abstract. **Using pulses of multifrequency stimulated Raman scattering (SRS) in calcite, nonlinear photoluminescence in a stilbene molecular crystal is excited. When multifrequency SRS is excited by the radiation of a Nd^{3+}:YAG laser with a wavelength of 1064 nm, eleven anti-Stokes components are observed in the visible spectrum with an average frequency shift of 1086 cm^{-1} between them. Using the second harmonic of the Nd^{3+}:YAG laser radiation allowed three anti-Stokes and four Stokes components to be recorded. The large spectral range of the frequency comb facilitated effective reduction in the duration and increase in the intensity of the radiation pulse of multifrequency SRS.**

Keywords: *calcite, stimulated Raman scattering, frequency comb, crystal, spontaneous Raman scattering, nonlinear photoluminescence, stilbene.*

1. Introduction

At a sufficiently high intensity of exciting radiation in a Raman-active dielectric medium, the process of stimulated Raman scattering of light (SRS) can occur. SRS processes in dielectric media have been actively studied since the middle of the last century [1–4]. An increase in the intensity of exciting radiation makes it possible to realise multifrequency four-photon parametric processes. In the elementary act of such processes, two quanta of exciting radiation are simultaneously absorbed and the complementary Stokes and anti-Stokes SRS satellites appear simultaneously. A further increase in the intensity of exciting radiation leads to the appearance of a comb of SRS frequencies, occupying a large spectral range in the Stokes and anti-Stokes regions. The theoretical analysis of the generation of collinear optical components at multifrequency SRS and the processes of conversion of monochromatic laser radiation into a comb of equidistant frequencies in the IR and visible spectral regions was considered in Refs [5, 6]. In Ref. [7], for SRS in a calcite crystal the matching conditions of the four-wave parametric processes, characterised by a rather low threshold, were investigated theoretically and experimentally. From the theoretically derived dependences, it follows that the use of bichromatic pumping leads to broadening of the scattered radiation spectrum and the generation of many Raman components in the process of SRS [8].

The calcite crystal is a widely known dielectric crystal with a relatively high SRS gain [9]. The refractive indices of the birefringent $CaCO_3$ single crystal are 1.658 for the ordinary ray and 1.486 for the extraordinary ray [9]. The Raman gain in the calcite crystal pumped by the second harmonic of a Nd^{3+}:YAG laser radiation is 13 cm GW^{-1} for an ordinary beam [10].

Spontaneous Raman scattering (RS) in calcite crystals was studied in Refs [11–13]. The vibrational spectrum of this crystal was also studied using IR spectroscopy [11, 14]. The full spectrum of spontaneous Raman scattering consists of five fundamental lines and one combination line. A narrow line corresponding to a totally symmetrical vibration with the frequency ν = 1086 cm^{-1} has the highest intensity in the Raman spectrum. The calculated lifetimes for weaker low frequency (lattice) modes with frequencies of 155, 282, and 303 cm^{-1} are 1.6 ps, 1.3 ps, and 250 fs, respectively [15]. The Raman spectrum of calcite crystals differs significantly from the spectra of carbonates (aragonite and dolomite) in the frequencies of their fundamental modes [16–20]. Methods have been developed that allow calculating the concentration of artificial calcite crystals in a mixture of its polymorphic modifications from Raman spectra [21].

The relatively high SRS gain in the calcite crystal and the availability of this crystal caused its widespread use for the development of Raman lasers. The calcite single crystal lengths under which optimal conditions are achieved for the parametric coupling between the Stokes and anti-Stokes components and the generation of higher Raman satellites are 9–13 mm and 3–8 mm, when excited by laser radiation with wavelengths of 1064 and 532 nm, respectively [22]. The edge of the widest frequency comb of anti-Stokes SRS components in a calcite crystal using the fundamental line of the Nd^{3+}:YAG laser corresponded to a wavelength λ = 341.5 nm [23]. In this case, the third optical harmonic was recorded at λ = 354.7 nm. The generation of multifrequency parametric Raman scattering was also observed in other nonlinear optical crystals: in aragonite [24], $Ba(NO_3)_2$ [25], diamond [26], BaF_2 [27], etc. With high-intensity repetitively pulsed excitation by Nd^{3+}:YAG laser radiation in protium and deuterium water, several Raman satellites were detected in SRS [28]. It was found that upon resonance excitation of sodium nitrite crystals by the radiation of a nitrogen laser (λ = 337 nm), a large number of equidistant lines are also present in the spectrum of secondary radiation [29].

When intense laser radiation was used as a pump in the transparency region of a dielectric, a number of papers [30, 31] reported the observation, in addition to the SRS processes, of

V.S. Gorelik, A.V. Skrabatun Lebedev Physical Institute, Russian Academy of Sciences, Leninsky prosp. 53, 119991 Moscow, Russia; Bauman Moscow State Technical University, Vtoraya Baumanskaya ul. 5, stroenie 1, 105005 Moscow, Russia; e-mail: skrabatunav@lebedev.ru; **V.A. Orlovich, A.I. Vodchits** B.I. Stepanov Institute of Physics, National Academy of Sciences of Belarus, prosp. Nezavisimosti 68, 220072 Minsk, Belarus

Received 25 November 2019; revision received 13 February 2020
Kvantovaya Elektronika **50** (7) 700–706 (2020)
Translated by V.L. Derbov

two-photon-excited luminescence (TPEL). In particular, the study of the TPEL in compounds with aromatic groups (fluorene, anthracene, paraterphenyl, and stilbene) was performed in [32] upon excitation by ~10-ns radiation pulses of a repetitively pulsed copper vapour laser. The TPEL spectra of stilbene microcrystals were also studied upon excitation by radiation of a Nd^{3+}:YAG laser. It was found that in the stilbene molecular crystal, there is a transition from the spontaneous TPEL regime to the superluminescence regime, when the pump radiation intensity reaches 10^8 W cm^{-2} [33]. The specific features of two-photon processes in a stilbene crystal and the results of numerical simulation of the TPEL spectrum were analysed in [34].

The aim of this work was to study the conditions for the excitation of TPEL in a stilbene molecular crystal using the comb of SRS frequencies as a pump. To generate a frequency comb in the visible and near-IR ranges, we used multifrequency Raman scattering in a calcite single crystal excited by ultrashort pulses from a solid-state Nd^{3+}:YAG laser with wavelengths of 1064 and 532 nm.

2. Theory

$CaCO_3$ crystallises into a trigonal structure with a space symmetry group $D^6_{3d}(R\bar{3}c)$ [11, 35], forming a rhombohedron with two molecules in a primitive cell (Fig. 1). Calcium and carbon ions are located on the trigonal axis, and both carbonate ions are located so that there is a centre of inversion. Calcite cations are in position with S_6 symmetry. Anions form two groups of atoms, which can be limited by triangular D_3 symmetry planes. The principal diagonal of the rhombohedron is the third-order symmetry axis (C_3). The planes bounding the CO_3^{2-} groups are perpendicular to the principal axis of the rhombohedron and rotated by 60° relative to each other. The unperturbed negative carbonate ion CO_3^{2-} (D_{3h} symmetry) has the following internal vibrations: a symmetric Raman-active mode $\nu_1(A_1')$ with an energy of 1086 cm^{-1}, a deformation IR-active mode $\nu_2(A_2'')$ with an energy of about 825 cm^{-1}, and Raman- and IR-active vibrations with frequencies $\nu_3(E')$ and $\nu_4(E'')$ with energies of 1436 and 711 cm^{-1}, respectively [11].

The calcite primitive cell contains ten atoms, which are characterised by 27 optical irreducible representations of the point symmetry group D_{3d}. Table 1 shows the results of a group-theoretical analysis of a calcite crystal [11, 36] belonging to the space group D^6_{3d}.

The T_{opt} representation contains the full spectrum of optical vibrations of the calcite crystal, which can be decomposed into the following components: $T_{opt} = T_{tr} + T_{lib} + T_{in}$. Here, T_{tr} corresponds to translational lattice modes (translational vibrations of the Ca atom), T_{lib} to librations of the CO_3^{2-} group, and T_{in} to intramolecular (internal) vibrations of the CO_3^{2-} group. According to the selection rules [37], IR absorption is allowed for vibrations $V = A_{2u} + E_u$, and Raman scattering is allowed for symmetric vibrations $[V]^2 = 2A_{1g} + E_g$. In Table 1, the activity of modes in IR emission or in Raman scattering is indicated in parentheses. Thus, in the Raman spectrum two lines corresponding to the lattice modes and located in its low-frequency region should be observed. High-frequency vibrations corresponding to internal oscillations of the carbonate group should manifest themselves in the form of three bands.

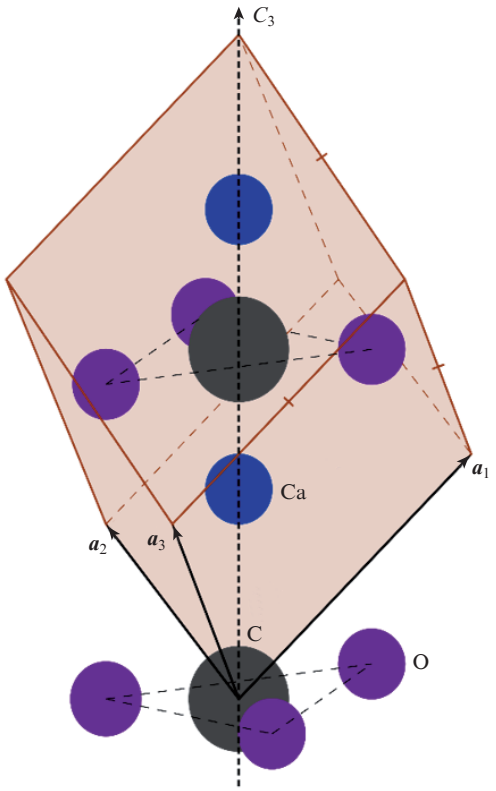

Figure 1. Calcite crystal primitive cell.

3. Experimental technique

The spectra of spontaneous Raman scattering in the calcite single crystal were recorded using an experimental setup, described in Ref. [25]. The excitation source was a cw laser with a wavelength of 785 nm and a power of 200 mW. The spectral resolution of the BWS465-785H spectrometer was 3.5 cm^{-1}.

To excite multifrequency SRS, a Nd^{3+}:YAG laser with the fundamental line wavelength of 1064 nm was used as a radiation source. When a nonlinear optical crystal was installed in the laser cavity, the second optical harmonic was generated with λ = 532 nm. The laser generated pulses with durations of 80 and 60 ps and a repetition rate of 20 Hz using the fundamental and second harmonics, respectively. The maximum laser pulse energy reached 24 and 60 mJ, and the radiation power was 0.3 and 1.0 GW for λ = 1064 and 532 nm, respectively. The calcite crystal used was cut along the princi-

Table 1. Results of a group-theoretical analysis of a calcite crystal belonging to the space symmetry group D^6_{3d}.

Representation	Classification of vibrations	Number of Raman-active modes
T_{opt}	$A_{1g}(RS) + 3A_{2g} + 4E_g(RS) + 2A_{1u} + 3A_{2u}(IR) + 5E_u(IR)$	5
T_{tr}	$A_{2g} + E_g(RS) + A_{1u} + A_{2u}(IR) + 2E_u(IR)$	1
T_{lib}	$A_{2g} + E_g(RS) + A_{2u}(IR) + E_u(IR)$	1
T_{in}	$A_{1g}(RS) + A_{2g} + 2E_g(RS) + A_{1u} + A_{2u}(IR) + 2E_u(IR)$	3

pal crystallographic axis C_3. When laser radiation was focused inside the studied dielectric, the maximum intensity was ~100 GWcm^{-2}. According to the results of Ref. [22], when the second optical harmonic of a Nd^{3+}:YAG laser with λ = 532 nm and a pulse duration of 20 ps is used to stimulate SRS, the radiation resistance threshold of the $CaCO_3$ crystal is 1.4 TWcm^{-2}, i.e., in our experiments the SRS spectra were recorded in a nondestructive regime for the studied crystals.

Figure 2 schematically shows the experimental setup used to observe multifrequency SRS in calcite. The radiation of a laser (*1*) after passing through a semitransparent plate (*2*) is incident on a plano-convex lens (*4*) adjacent to the surface of the sample. A calcite crystal (*5*) is placed between two lenses (*4*), as a result of which the laser radiation intensity on the surface of the calcite crystal is significantly lower than inside the sample. The multifrequency SRS signal is focused by a lens (*3*) into the fibre holder and through a single-core fibre (*6*) is fed to a FSD-8 spectrometer (*7*) connected to a computer (*8*). The multifrequency SRS also propagates in the backward direction. To record this radiation, after the semitransparent plate (*2*), an additional quartz lens (*3*), optical fibre (*6*), spectrometer (*7*), and computer (*8*) are installed. The FSD-8 spectrometer, using a multi-element detector, ensures the registration of spectra in a wide spectral range (200–1000 nm) with exposures from 100 μs up to 32 s. The spectral resolution is about 1 nm. The focal length of plano-convex lenses is 20 mm.

The setup for observing multifrequency SRS and TPEL pumped by the second harmonic of the Nd^{3+}:YAG laser with λ = 532 nm is shown in Fig. 3. The multifrequency SRS signal from the calcite crystal (*5*) is focused by a lens (*3*) into a cuvette (*7*) filled with a 3 mm-thick layer of microcrystalline stilbene powder (*8*). The second-harmonic radiation of the Nd^{3+}:YAG laser and multifrequency SRS excites TPEL in the stilbene microcrystals. The SRS and TPEL signals are directed through optical fibres (*9*) to a FSD-8 mini-spectrometers (*10*) and computers (*11*) connected to them. The radiation of multifrequency SRS propagates in the forward and backward directions. To suppress the high- intensity radiation of the laser source, a cutoff filter (*12*) is installed on the return path.

4. Results and discussion

The recorded spontaneous Raman spectra in a calcite single crystal upon excitation by a cw laser with λ = 785 nm are shown in Fig. 4. The full spectrum obtained consisted of six main narrow lines (Table 2). In the high-frequency region of the spectrum, a low-intensity band was observed in the fre-

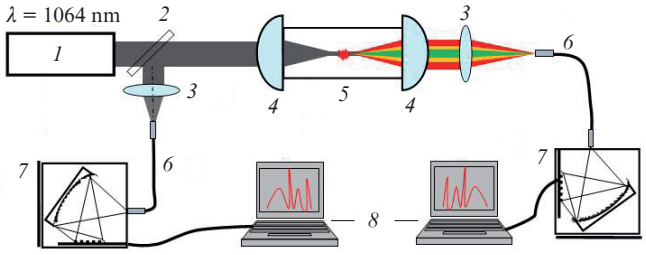

Figure 2. Schematic of the experimental setup with a Nd^{3+}:YAG laser for observing multifrequency SRS: (*1*) radiation source; (*2*) semitransparent plate; (*3*) focusing lenses; (*4*) plano-convex lenses; (*5*) calcite single crystal; (*6*) single-core optical fibres; (*7*) spectrometers; (*8*) computers.

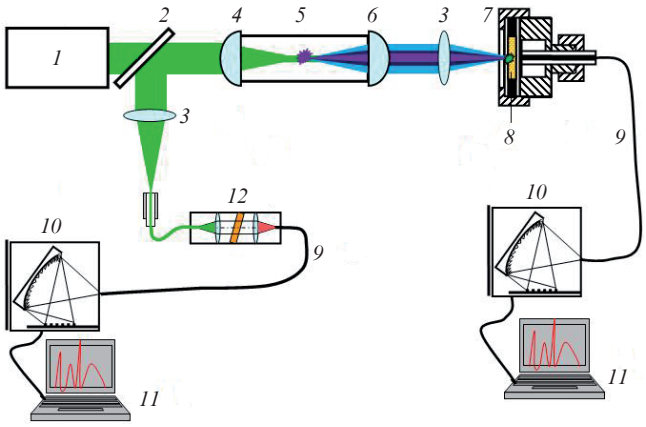

Figure 3. Schematic of the experimental setup for observing nonlinear luminescence and multifrequency SRS using the second harmonic of a Nd^{3+}:YAG laser as exciting radiation:
(*1*) radiation source; (*2*) semitransparent plate; (*3*) focusing lenses; (*4*, *6*) plano-convex lenses; (*5*) calcite single crystal; (*7*) cuvette; (*8*) stilbene microcrystals; (*9*) single-core optical fibres; (*10*) mini-spectrometers; (*11*) computers; (*12*) cutoff filter.

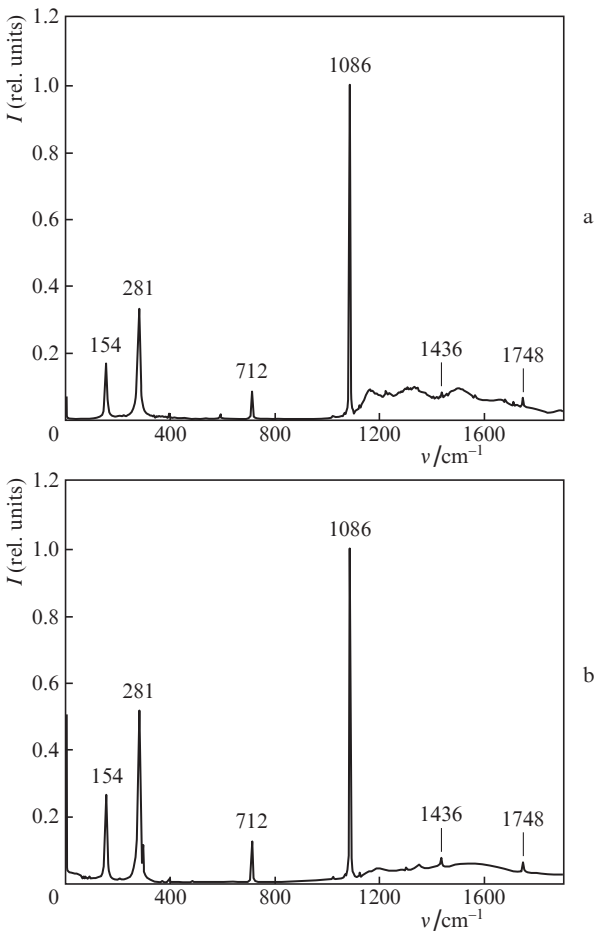

Figure 4. Normalised spectra of spontaneous Raman scattering in a calcite crystal, recorded for directions of exciting radiation (a) along and (b) across the principal axis of the rhombohedron (C_3). The exposure time was (a) 200 and (b) 400 s.

Table 2. Vibration frequencies and the corresponding symmetry species in the spectrum of spontaneous Raman scattering in calcite recorded at room temperature.

ν/cm^{-1}	Vibration D_{3d}^{6} symmetry species	Vibration type
154	E_g	Lattice modes
281	E_g	
712	E_g	
1086	A_{1g}	Internal modes
1436	E_g	
1748	A_{1g}; E_g	

quency range ν = 1200–1800 cm^{-1} and weak peaks corresponding to the fundamental mode E_g (ν = 1436 cm^{-1}) and a combination of the A_{1g} and E_g modes (ν = 1748 cm^{-1}). The frequencies of spontaneous Raman lines shown in Table 2, according to the results of Refs [11, 35, 38], were correlated with the corresponding types of symmetry.

Table 2 also presents different types of vibrations: low-frequency lattice vibrations and high-frequency internal ones. The line with the frequency ν = 1086 cm^{-1} , which corresponds to the internal vibrations of the carbonate group, had the highest intensity in the spectrum of spontaneous Raman scattering. The half-width of this line was 2.0 cm^{-1}. A wide band in the range ν = 1200–1800 cm^{-1} is the result of the excitation of two-phonon states of a calcite single crystal by cw laser radiation.

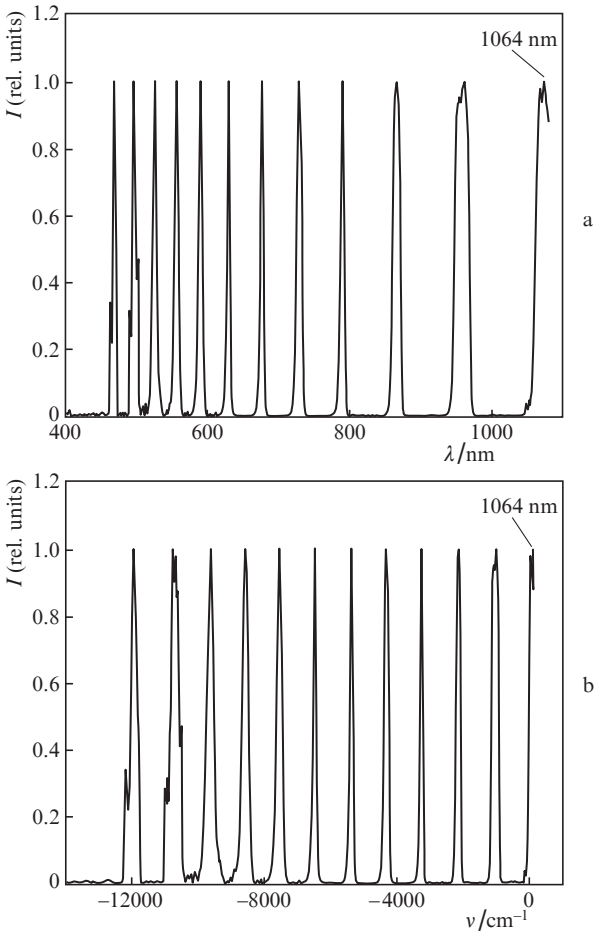

Figure 5. Normalised spectra of multifrequency anti-Stokes SRS in calcite as a function of (a) wavelength and (b) frequency shift ν, obtained upon excitation of the crystal by repetitively pulsed laser radiation with λ = 1064 nm.

Figure 5 shows the anti-Stokes multifrequency Raman spectra excited in a calcite single crystal by repetitively pulsed radiation from a Nd^{3+}:YAG laser with λ = 1064 nm. A large number of Raman satellites were observed in the near-IR and visible spectral regions. Each SRS line was normalised to unity for more accurate determination of half-widths and line frequencies. Wavelengths of lines and frequency separations $|\Delta\nu|$ between them are given in Table 3.

According to Fig. 5 and the data in Table 3, eleven anti-Stokes (ASt) satellites with A_{1g} symmetry were observed in the spectrum of multifrequency SRS, shifted in frequency relative to each other by an average of ν = 1086 cm^{-1}. Figure 6 shows the dependences of the half-widths $\delta\nu$ of the satellites and their frequency shifts $|\Delta\nu|$ upon the anti-Stokes component number N.

Table 3. Wavelengths of observed anti-Stokes SRS satellites in calcite and frequency distances $|\Delta\nu|$ between them when using a laser source with λ = 1064 nm (the accuracy of measuring the frequencies $|\Delta|$ with the spectrometer resolution taken into account is 50 cm^{-1}).

Raman satellite wavelength/nm	$\lvert\Delta\nu\rvert$ /cm^{-1}	Satellite notation
467	1183	ASt 11
496	1153	ASt 10
526	1038	ASt 9
556	1020	ASt 8
590	1071	ASt 7
630	1099	ASt 6
677	1047	ASt 5
728	1069	ASt 4
790	1114	ASt 3
866	1071	ASt 2
955	1074	ASt 1
1064	–	–

It can be seen from Fig. 6a that, starting from the fifth anti-Stokes satellite, the half-widths of the lines monotonically increase towards the short-wavelength region of the spectrum. The obtained points were approximated by a third-order polynomial. The eleventh Raman satellite was not considered because of its low intensity and low accuracy of determining its half-width. In Fig. 6b, the frequency shift within the measurement error was unchanged for the first nine SRS satellites and corresponded to the value given in the literature [22, 23]. An increase in the half-widths of the Raman satellites (Fig. 6a) caused an increase in the error in measuring their frequencies (Fig. 6b).

Raman satellites correspond to the energy and momentum conservation laws characteristic for parametric four-wave mixing:

$$\begin{aligned} &2\hbar\omega_p = \hbar\omega_{ASt1} + \hbar\omega_{St1}, \quad 2\hbar\boldsymbol{k}_p = \hbar\boldsymbol{k}_{ASt1} + \hbar\boldsymbol{k}_{St1}, \\ &2\hbar\omega_p = \hbar\omega_{ASt2} + \hbar\omega_{St2}, \quad 2\hbar\boldsymbol{k}_p = \hbar\boldsymbol{k}_{ASt2} + \hbar\boldsymbol{k}_{St2}, \\ &\ldots\ldots\ldots\ldots\ldots\ldots\ldots\ldots\ldots\ldots\ldots\ldots\ldots\ldots\ldots\ldots\ldots\ldots \\ &2\hbar\omega_p = \hbar\omega_{ASt8} + \hbar\omega_{St8}, \quad 2\hbar\boldsymbol{k}_p = \hbar\boldsymbol{k}_{ASt8} + \hbar\boldsymbol{k}_{St8}. \end{aligned} \tag{1}$$

Here, the subscript p refers to pump radiation.

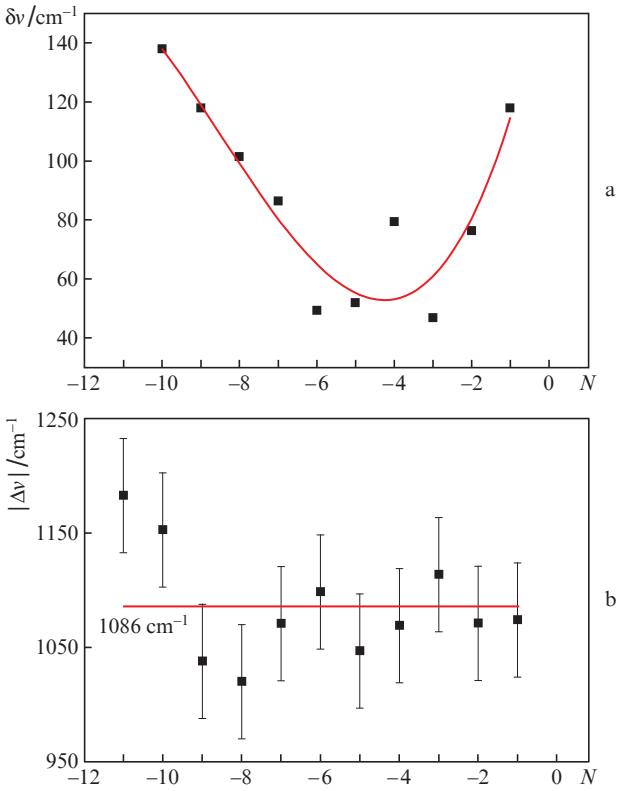

Figure 6. Dependences of (a) the half-widths $\delta\nu$ of Raman satellites and (b) their frequency shifts $|\Delta\nu|$ on the anti-Stokes satellite number N.

As can be seen from Fig. 5a, the ninth Raman satellite with $\lambda = 526$ nm ($\nu = 19011$ cm^{-1}) had a frequency higher than the second harmonic frequency of the pump radiation $2\nu = 18796$ cm^{-1} ($\lambda = 532$ nm). SRS generation at frequencies exceeding the overtone frequency $2\nu = 18796$ cm^{-1} ($\lambda = 532$ nm) of laser radiation at $\lambda = 1/\nu = 1064$ nm indicates a cascade mechanism for the generation of the ninth, tenth, and eleventh Raman components. In this case, the laws of energy and momentum conservation take the form:

$$2\hbar\omega_{ASt9} = \hbar\omega_{ASt8} + \hbar\omega_{ASt10},\ 2\hbar\boldsymbol{k}_{ASt9} = \hbar\boldsymbol{k}_{ASt8} + \hbar\boldsymbol{k}_{ASt10},$$

$$2\hbar\omega_{ASt10} = \hbar\omega_{ASt11} + \hbar\omega_{ASt9},\ 2\hbar\boldsymbol{k}_{ASt10} = \hbar\boldsymbol{k}_{ASt11} + \hbar\boldsymbol{k}_{ASt9}, \quad (2)$$

$$2\hbar\omega_{ASt11} = \hbar\omega_{ASt12} + \hbar\omega_{ASt10},\ 2\hbar\boldsymbol{k}_{ASt11} = \hbar\boldsymbol{k}_{ASt12} + \hbar\boldsymbol{k}_{ASt10}.$$

The fulfillment of the momentum conservation law in elementary four-photon processes (1) and (2) led to the observed angular dependences of the intensities of individual SRS components. The phase-matching condition in this work could be achieved at the expense of violating the momentum conservation law due to the presence of impurities and defects in a real crystal. A confirmation of this assumption is the presence of a relaxation central peak in the low-frequency Raman spectrum observed, e. g., in a quartz crystal [39].

Figure 7 shows the spectrum of multifrequency SRS in a calcite single crystal obtained upon excitation of scattering by second-harmonic radiation from a repetitively pulsed Nd^{3+}:YAG laser. The spectrum contains four Stokes and

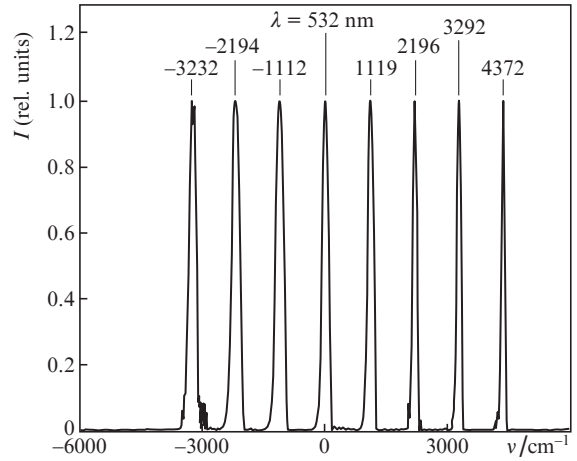

Figure 7. Normalised spectrum of multifrequency SRS in calcite excited by a Nd^{3+}:YAG laser with $\lambda = 532$ nm.

three anti-Stokes satellites with an average frequency shift between them of 1086 cm^{-1} (with the spectrometer resolution taken into account, the measurement accuracy is $|\Delta| = 50$ cm^{-1}). The wavelengths of the satellites and the frequency separations between them are given in Table 4. The frequency shifts between the adjacent Stokes (St) and anti-Stokes components did not undergo significant changes in the entire spectral range. The frequency separations between all Raman satellites in Table 4 correspond to the internal A_{1g} mode of the calcite crystal.

Table 4. Wavelengths of observed anti-Stokes SRS satellites in calcite and frequency distances $|\Delta\nu|$ between them under excitation by a laser source with $\lambda = 532$ нм (the accuracy of measuring the frequencies $|\Delta|$ with the resolution of the spectrometer taken into account, is 50 cm^{-1}).

Raman satellite wavelength/nm	$\lvert\Delta\nu\rvert$/cm^{-1}	Satellite notation
454	1038	ASt 3
476	1082	ASt 2
502	1112	ASt 1
532	–	–
565	1119	St 1
602	1077	St 2
645	1096	St 3
693	1080	St 4

Figure 8 shows the TPEL spectra in stilbene microcrystals and multifrequency SRS in a calcite single crystal, obtained in experiments using the scheme of Fig. 3 and the second harmonic of a Nd^{3+}:YAG laser as excitation source. It can be seen that the spectrum in the wavelength range $\lambda = 414-564$ nm consists of the Stokes and anti-Stokes components of SRS in the calcite single crystal (the frequency shift between them is 1086 cm^{-1}). In addition, in the short-wavelength region of the spectrum, TPEL was excited in stilbene microcrystals simultaneously with SRS. Such a hybrid form of radiation can be classified as nonlinear photoluminescence. In this case, one Stokes and five anti-Stokes lines were observed in the spectrum of multifrequency SRS. The nonlinear photoluminescence of stilbene microcrystals in the range $\lambda = 360-410$ nm was excited by the radiation of multifrequency SRS in calcite. The duration of the multifrequency SRS signal

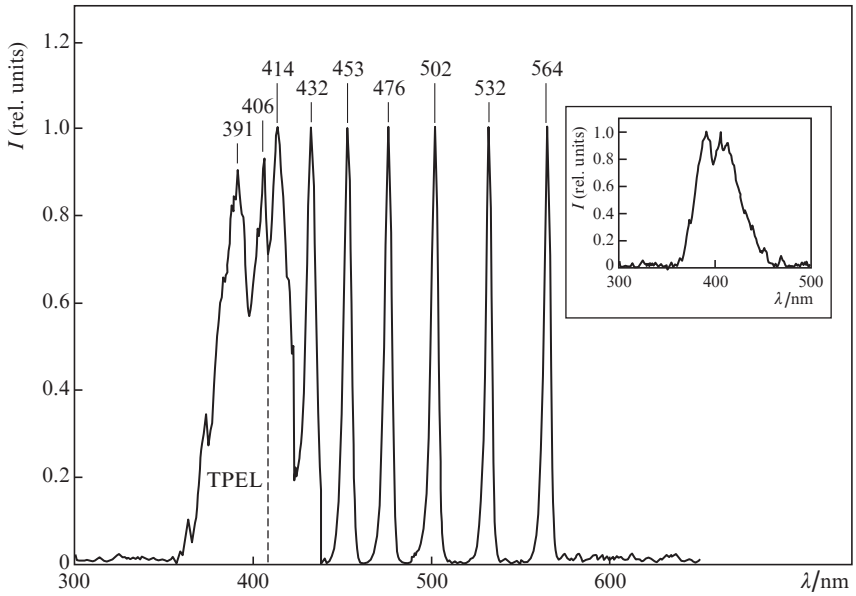

Figure 8. Normalised spectra of multifrequency SRS in a single crystal of calcite and TPEL in stilbene microcrystals excited by a Nd^{3+}:YAG laser with a wavelength $\lambda = 532$ nm. The inset shows the form of the TPEL spectrum in stilbene excited by picosecond (60 ps) repetitively pulsed radiation from a Nd^{3+}:YAG laser ($\lambda = 532$ nm).

was much shorter than the pulse duration of the exciting laser radiation with $\lambda = 532$ nm due to the significantly wider SRS spectrum. As a result, the nonlinear photoluminescence signal was amplified in stilbene. The nonlinear photoluminescence spectrum comprised intensity maxima at $\lambda = 391$ and 406 nm (Fig. 8a) and low-intensity peaks in the range 360–390 nm. The shape of the TPEL band recorded in [32] with excitation by radiation of a repetitively pulsed copper vapour laser, was close to the shape of the band obtained in this work, but shifted to the short-wavelength region. A small shift (by 10–15 nm) of the TPEL band to the long-wavelength region as compared with the data of Ref. [32] is explained by the fact that we used the 'transmission' scheme. In this case, the TPEL intensity decreases in the region of strong stilbene absorption when secondary radiation passes through the crystal layer 3 mm thick, while in Ref. [32] the TPEL spectra were recorded using the 'reflection' scheme.

5. Conclusions

Thus, in the present work, detailed spectra of spontaneous Raman scattering of calcite were recorded using a laser at 785 nm as a source of excitation. A broad band was revealed in the high-frequency region of these spectra, indicating the manifestation of two-phonon processes. When SRS was excited in a $CaCO_3$ crystal by radiation from a picosecond repetitively pulsed Nd^{3+}:YAG laser with $\lambda = 1064$ nm, multifrequency anti-Stokes SRS was observed in the near-IR and visible spectral ranges. Eleven anti-Stokes satellites corresponding to fully symmetric modes of the carbonate group were recorded with a frequency shift of $\sim$1086 cm^{-1} between them. As we move into the short-wavelength region of the spectrum, the frequency shift between adjacent anti-Stokes satellites changes, which may be due to an increase in their half-widths.

We recorded the nonlinear photoluminescence spectrum of stilbene, excited by radiation of multifrequency SRS in a calcite crystal pumped by laser radiation with $\lambda = 532$ nm. In this case, five anti-Stokes components of SRS were observed. The use of multifrequency SRS pulses can be promising for the conversion of IR radiation into the visible spectral region and the development of new methods for exciting nonlinear optical processes [40–43], in particular TPEL.

Acknowledgements. This work was supported by the Russian Foundation for Basic Research (Grant Nos 18-02-00181, 18-32-00259, and 20-52-00002).

References

1. Chiao R., Stoichefft B.P. *Phys. Rev. Lett.*, **12**, 290 (1964).
2. Woodbury E.J., Ng W.K. *Proc. IRE*, **50**, 2367 (1962).
3. Shen Y.R. *Light Scattering in Solids 1* (Berlin: Springer, 1983).
4. Sokolovskaya A.I., Kudryavtseva A.D., Brekhovskikh G.L., Sushchinskiy M.M. *Sov. Phys. J. Exp. Theor. Phys.*, **30**, 633 (1970) [*Zh. Eksp. Teor. Fiz.*, **57**, 1160 (1970)].
5. Lisinetskiy V.A., Bus'ko D.N., Chulkov R.V., Grabchikov A.S., Apanasevich P.A., Orlovich V.A. *Zh. Prikl. Spektrosk.*, **75**, 284 (2008).
6. Smetanin S.N. *Quantum Electron.*, **44**, 1012 (2014) [*Kvantovaya Elektron.*, **44**, 1012 (2014)].
7. Smetanin S.N., Fedin A.V., Shurygin A.S. *Quantum Electron.*, **43**, 512 (2013) [*Kvantovaya Elektron.*, **43**, 512 (2013)].
8. Kochanov V.P. *J. Exp. Theor. Phys.*, **128**, 14 (2019) [*Zh. Eksp. Teor. Fiz.*, **155**, 20 (2019)].
9. Long L.L., Querry M.R., Bell R.J., Alexander R.W. *Infrared. Phys.*, **34**, 191 (1993).
10. Karpukhin S.N., Stepanov A.I. *Sov. J. Quantum Electron.*, **16**, 1927 (1986) [*Kvantovaya Elektron.*, **13**, 1572 (1986)].
11. Gunasekaran S., Anbalagan G., Pandi S. *J. Raman Spectrosc.*, **37**, 892 (2006).
12. Tlili M.M., Amor M.B., Gabrielli C., Joiret S., Maurin G., Rousseau P. *J. Electrochem. Soc.*, **150**, 485 (2003).
13. Pierre M., Carteret C., Maschio L., André E., Orlando R., Dovesi R. *J. Chem. Phys.*, **140**, 164509 (2014).
14. Andersen F.A., Brecevic L. *Acta Chem. Scand.*, **45**, 1018 (1991).
15. Wang L., Liu W., Fang C. *Phys. Chem. Chem. Phys.*, **17**, 17034 (2015).
16. Edwards H.G.M., Villar S.E.J., Jehlicka J., Munshi T. *Spectrochim. Acta, Part A*, **61**, 2273 (2005).
17. Herman R.G., Bogdan C.E., Sommer A.J., Simpson D.R. *Appl. Spectrosc.*, **41**, 437 (1987).

18. Prencipe M., Pascale F., Zicovich-Wilson C.M., Saunders V.R., Orlando R., Dovesi R. *Phys. Chem. Miner.*, **31**, 559 (2004).
19. Valenzano L., Noël Y., Orlando R., Zicovich-Wilson C.M., Ferrero M., Dovesi R. *Theor. Chem. Acc.*, **117**, 991 (2007).
20. Valenzano L., Torres F.J., Doll K., Pascale F., Zicovich-Wilson C.M., Dovesi R.Z. *Phys. Chem.*, **220**, 893 (2006).
21. Ševčík R., Mácová P. *Vib. Spectrosc.*, **95**, 1 (2018).
22. Smetanin S.N., Jelinek M. Jr., Kubeček V., Jelinkova H. *Laser Phys. Lett.*, **12**, 095403 (2015).
23. Kaminskii A.A., Bohatý L., Becker P., Eichler H.J., Rhee H. *Laser Phys. Lett.*, **7**, 142 (2010).
24. Kaminskii A.A., Rhee H., Lux O., Eichler H.J., Koltashev V.V., Kleinschrodt R., Bohatý L., Becker P. *Laser Phys. Lett.*, **9**, 259 (2012).
25. Gorelik V.S., Skrabatun A.V., Orlovich V.A., Voinov Yu.P., Vodchits A.I., Pyatyshev A.Yu. *Quantum Electron.*, **49**, 231 (2019) [*Kvantovaya Elektron.*, **49**, 231 (2019)].
26. Lux O., Ralchenko V.G., Bolshakov A.P., Konov V.I., Sharonov G.V., Shirakawa A., Yoneda H., Rhee H., Eichler H.J., Mildren R.P., Kaminskii A.A. *Laser Phys. Lett.*, **11**, 086101 (2014).
27. Kaminskii A.A., Rhee H., Eichler H.J., Bohatý L., Becker P., Takaichi K. *Laser Phys. Lett.*, **5**, 304 (2008).
28. Gorelik V.S., Bi Dongxue, Voynov Yu.P., Vodchits A.I., Orlovich V.A., Savel'yeva A.I. *Opt. Spectrosc.*, **126**, 533 (2019) [*Opt. Spektrosk.*, **126**, 765 (2019)].
29. Gorelik V.S., Lepnev L.S., Pyatyshev A.Yu., Skrabatun A.V. *Neorg. Mater.*, **53**, 49 (2017).
30. Becker C., Burger S., Barth C., Manley P., Jäger K., Eisenhauer D., Köppel G., Chabera P., Chen J., Zheng K., Pullerits T. *ACS Photonics*, **5**, 4668 (2018).
31. Loumaigne M., Vasanthakumar P., Richard A., Derbarre A. *Phys. Chem. Chem. Phys.*, **13**, 11597 (2011).
32. Gorelik V.S., Zhabotinskii E.V. *J. Russ. Laser Res.*, **16**, 287 (1995).
33. Gorelik V.S., Sokolovskaya A.I., Chernega N.V., Shcheglov V.A. *Quantum Electron.*, **23**, 505 (1993) [*Kvantovaya Elektron.*, **20**, 586 (1993)].
34. Wergifosse M., Elles C.G., Krylov A.I. *J. Chem. Phys.*, **146**, 174102 (2017).
35. Behrens G., Kuhn L.T., Ubic R., Heuer A.H. *Spectrosc. Lett.*, **28**, 983 (1995).
36. Rutt H.N., Nicola J.H. *J. Phys. C: Solid State Phys.*, **7**, 4522 (1974).
37. Zhizhin G.N., Mavrin B.N., Shabanov V.F. *Opticheskie kolebatel'nye spektry kristallov* (Optical Vibrational Spectra of Crystals) (Moscow: Nauka, 1984).
38. Kontoyannis C.G., Vagenas N.V. *Analyst*, **125**, 251 (2000).
39. Gorelik V.S., Pyatyshev A.Yu. *J. Raman Spectrosc.*, **50**, 1584 (2019).
40. Kumar A., Gupta P.S. *Quantum Semiclassical Opt.*, **7**, 835 (1995).
41. Giri D.K., Gupta P.S. *J. Opt. B: Quantum Semiclassical Opt.*, **6**, 91 (2004).
42. Perina J., Krepelka J. *J. Mod. Opt.*, **38**, 2137 (1991).
43. Kumar A., Gupta P.S. *Quantum Semiclassical Opt.*, **8**, 1053 (1996).